Polarized Compton scattering from ^{4}He in the Δ region

V. Bellini,[1,2] M. Capogni,[3,4,*] A. Caracappa,[5] L. Casano,[3] A. D'Angelo,[3,4] F. Ghio,[6,7] B. Girolami,[6,7] S. Hoblit,[8] L. Hu,[3] M. Khandaker,[9] O. C. Kistner,[5] L. Miceli,[5] D. Moricciani,[3] A. M. Sandorfi,[5] C. Schaerf,[3,4] and C. E. Thorn[5]

[1]*Dipartimento di Fisica dell'Universitá di Catania, Corso Italia 57, I-95129, Catania, Italy*

[2]*Istituto Nazionale di Fisica Nucleare - Laboratori Nazionali del Sud, Via S. Sofia 44, I-95125, Catania, Italy*

[3]*Istituto Nazionale di Fisica Nucleare - Sezione di Roma II, Via della Ricerca Scientifica 1, I-00133, Rome, Italy*

[4]*Dipartimento di Fisica dell'Universitá di Roma, "Tor Vergata" Via della Ricerca Scientifica 1, I-00133, Rome, Italy*

[5]*Physics Department, Brookhaven National Laboratory, Upton, New York 11973, USA*

[6]*Istituto Superiore di Sanitá, Viale Regina Elena 299, I-00161, Rome, Italy*

[7]*Istituto Nazionale di Fisica Nucleare - Sezione Roma 1, Piazzale Aldo Moro 2, I-00185, Rome, Italy*

[8]*Physics Department, University of Virginia, Charlottesville, Virginia 22901, USA*

[9]*Physics Department, Virginia Polytechnic Institute & State University, Blacksburg, Virginia 24061, USA*

(Received 1 August 2003; published 19 November 2003)

Differential cross sections and beam asymmetries of Compton scattering from ^{4}He have been measured with linearly polarized photons in the energy range from 206 to 310 MeV. The quality of the results has the potential to provide strong constraints on the understanding of the reaction mechanism in the Δ resonance region. A phenomenological analysis of the experimental results has been performed fitting the data to a multipole expansion including dipole and quadrupole scatterings in the impulse approximation. Results indicate that quadrupole contributions should not be neglected to reproduce the general trend of the experimental results. Comparison with predictions from recent theoretical models shows that important discrepancies exist particularly at backward angles. The additional information carried by the incident photon spin increases the difficulty in achieving a comprehensive description of experimental data.

DOI: 10.1103/PhysRevC.68.054607 PACS number(s): 25.20.Dc, 21.10.Ft, 24.70.+s, 29.27.Hj

I. INTRODUCTION

Since photons are not strongly absorbed, elastic photon scattering from nuclei at intermediate energies has the potential for providing information on the modification of nucleon properties in nuclear matter.

In recent years there have been several attempts to describe Compton scattering from nuclei in the few-hundred MeV region. At energies above pion threshold, the elementary amplitude for $N \rightarrow \Delta$ excitation becomes very large with the result that scattering from single nucleons becomes the most important component. Particular interest lies in the investigation of nuclear medium corrections to the Δ-isobar characteristics due to kinematical effects such as Fermi motion, Pauli blocking of Δ decay, $\Delta - N$ binding, multiple scattering of intermediate pions, and coupling of the Δ to π absorption channels. These are expected to produce a shifting and broadening of the Δ peak. A recent analysis of π^0 photoproduction on ^{4}He, in the framework of distorted wave impulse approximation applied to the unitary isobar model, introduces a phenomenological Δ self-energy and provides a quantitative estimation of the Δ mass increase equal to 19 MeV and a width broadening of 66 MeV [1,2] in agreement with results from pion-nucleus scattering.

In the case of Compton scattering, in addition to the dominant resonant scattering process from single nucleons [3,4], different models have incorporated a variety of other effects, including meson exchange currents (MEC) [5], Δ modifications within the nuclear medium in the framework of Δ-hole models [6–13], and nonresonant terms such as mesonic and kinetic seagull amplitudes and Kroll-Ruderman terms [14].

While these have improved the description of existing data, significant discrepancies remain, particularly at large scattering angles (corresponding to large momentum transfers) suggesting that some fundamental contribution must be missing or poorly represented in the present understanding of the Compton scattering in the Δ region [5].

With linearly polarized photons it is possible to access two structure functions that contribute to the cross section:

$$\frac{d\sigma}{d\Omega}(E_\gamma, \vartheta_\gamma^{\text{c.m.}}, \varphi) = \frac{d\sigma}{d\Omega}_{unp}(E_\gamma, \vartheta_\gamma^{\text{c.m.}}) + P\hat{\Sigma}(E_\gamma, \vartheta_\gamma^{\text{c.m.}})\cos(2\varphi). \tag{1}$$

Here E_γ is the incoming laboratory photon energy, $\vartheta_\gamma^{\text{c.m.}}$ is the polar scattering angle in the center of mass reference frame (c.m.), φ is the azimuthal angle of the polarization vector of the photon, P is the degree of linear polarization of the incoming photon beam, $d\sigma/d\Omega_{unp} = \frac{1}{2}(d\sigma_{\|} + d\sigma_{\perp})$ is the unpolarized cross section, and $\hat{\Sigma} = \frac{1}{2}(d\sigma_{\|} - d\sigma_{\perp})$ is the polarization dependent cross section (the numerator of the beam asymmetry ratio); $d\sigma_{\|}$ and $d\sigma_{\perp}$ are the cross sections observed with the electric vector of the photon parallel and perpendicular to the reaction plane, respectively. The ratio of the two structure functions $\Sigma = \hat{\Sigma}/d\sigma/d\Omega_{unp}$ provides the beam asymmetry and it is very sensitive to

*Present address: ENEA-C.R. Casaccia, Via Anguillarese 301, I-00060, Santa di Galeria (RM), Italy.

interference effects that are easily masked in the unpolarized cross section and may provide new valuable constraints to theoretical models of the γ-nucleus interaction.

Among the spin-zero nuclei, ^{4}He has been an attractive target because of the large energy gap between the ground state and the continuum, and complex calculations are available. First data on coherent photon scattering from ^{4}He have been obtained using unpolarized Bremsstrahlung beams [15–19]. Compton events were extracted from the energy spectrum of a photon detector. The separation from the main background, π^0 production, was obtained considering the yield between photons scattered from the end-point of the Bremsstrahlung spectrum and the maximum photon energy from π^0 decay. The data analysis procedure had to rely on a very good knowledge of the photon detector response and on Monte Carlo simulations.

More precise data have been obtained at Mainz. A first measurement was performed with tagged photons at a fixed scattering angle $\theta_{lab}=37°$ [20]; more results were obtained with a tagged polarized beam from coherent Bremsstrahlung at three scattering angles [14]. Few data points with large error bars have been obtained for the beam polarization observable. The data analysis still required Monte Carlo simulation to properly subtract the background contribution from π^0 photoproduction events.

Complete separation of Compton events from background is desirable for studying the polarization dependent cross section because the azimuthal distribution of scattered photons has a minimum where the background π^0 production is maximum [21,22,14].

In this paper we present the complete and final set of results [23] from the measurement of Compton scattering on ^{4}He with tagged linearly polarized photons in the energy range 206–310 MeV and photon scattering angles between 30° and 130° in the laboratory frame.

The experimental setup is described in Sec. II and the data analysis procedure is shown in Sec. III. Final data are reported in Sec. IV together with a multipole fit of our full set of results with polarized photons.

Comparison with existing data and theoretical models is discussed in Sec. V, where conclusions are also summarized.

II. EXPERIMENTAL SETUP

The experiment was carried out at the laser electron gamma source (LEGS) facility located at the national synchrotron light source of Brookhaven National Laboratory [24]. Linearly polarized γ-rays were produced by backscattering laser light from 2.58-GeV electrons. Measurements for the polarized differential cross section were performed at 31, 45, 72.5, 90, 110, and 130 degrees for the polar angles of the scattered photons in the laboratory frame. The incoming photons were tagged with an energy resolution of 5 MeV full width at half maximum (FWHM). Events were collected in five γ energy bins with average values of 206, 224, 253, 282, and 310 MeV.

The beam polarization was alternatively set parallel and perpendicular to the reaction plane; the change among the two polarization states occurred after a time interval randomly selected between 5 and 10 min, in order to reduce systematic errors. Independent sets of data were taken at the same scattering angles, using two different laser lines that provided incoming photons in the energy ranges 206–240 MeV and 220–310 MeV, respectively. The photon beam polarization is strongly dependent on the ratio E_γ/E_γ^{Max}, where E_γ is the energy of the single photon of the incoming beam and E_γ^{Max} is the maximum energy available for the beam; the comparison among the data obtained at the same beam energy, but for different beam setup and polarizations, was used as a consistency check for the incoming photon beam properties (tagged photon flux and beam polarization).

Photons impinged on a 10-cm liquid ^{4}He target, contained in a thin electroformed Nickel cell. The target pressure and temperature were continuously monitored during the experiment to determine the density of the liquid, its average value being $\varrho=0.140\pm0.001$ g/cm^3.

The scattered photons were detected by a high resolution, cylindrical 48-cm $\phi\times48$ cm long NaI(Tl) scintillator (*main detector*). This crystal was surrounded by a 2.5-cm front plastic and an *annulus* of 12 plastic scintillators 10 cm thick, used to reject cosmic rays, charged particles, and electromagnetic shower leakage. A 21 cm diameter lead collimator was used to define the detector geometrical acceptance ($\Delta\Omega=0.13$ *sr*) and the whole apparatus was externally shielded with lead. The energy response function of this detector was measured at energies ranging from 212 to 316 MeV by placing it directly in the tagged photon beam. The energy resolution was about 2% FWHM and could be reduced to values as low as 1.5% FWHM by setting an appropriate threshold for the *annulus* scintillators in anticoincidence. The calibration, monitored several times during the data taking period (lasting about 2 months), was stable within 1%.

Eight NaI detector bars were placed in a *C* configuration around the target, covering a large solid angle with the opening in the direction of the *main detector*. These bars were used as vetoes against the competing processes (coherent π^0 photoproduction, photon scattering with ^{4}He breakup, and π^0 photoproduction with ^{4}He breakup). The described setup proved itself very effective in isolating Compton events.

Photomultiplier gains of all the detectors were continuously monitored by means of a laser pulse. Data acquisition was triggered by the coincidence between the tagger and the main detector, vetoed by any of the detectors surrounding the crystal. Accidental events subtraction was also performed using the time of flight (TOF) information between the trigger of the experiment and the tagger signals. Empty target runs were taken for each beam setup and photon scattering angle, in order to subtract background events produced on the nickel target ends and vacuum windows.

The beam flux N_γ was monitored using a γ converter quantameter, consisting of a sandwich of two plastic scintillators and a thin copper plate inserted between them, in coincidence with the 64 signals from the tagging scintillator counters. The monitor counts were normalized taking into account the detector efficiency, which was regularly measured using a 20-cm $\phi\times30$-cm NaI counter at low photon fluxes.

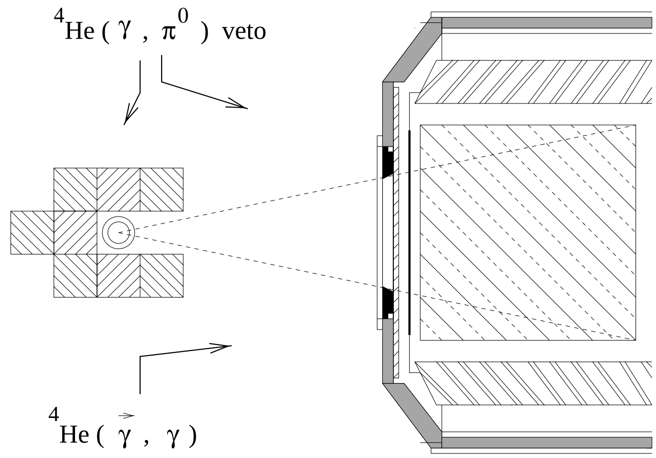

FIG. 1. Schematic view of the detector setup. A large 48 $\times$48 cm^2 NaI(TI) counter detects the scattered photons. A set of eight scintillating detectors is arranged in C configuration around the target; it was used to veto the additional photons from background π^0 decay.

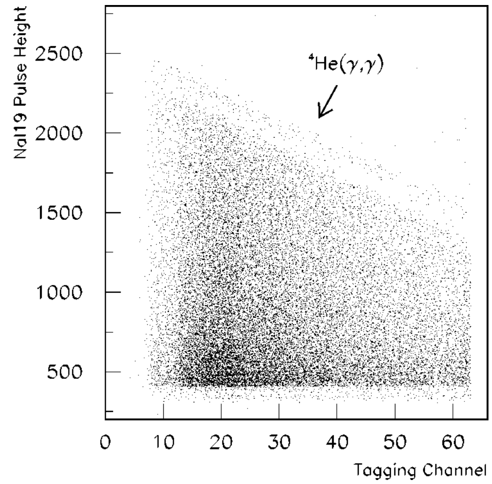

FIG. 2. Bi-dimensional plot of the scattered photon energy detected by the 48$\times$48 cm^2 NaI(Tl) counter (shown as pulse height) vs the incoming photon energy (shown as tagging channel). The upper band represents the Compton scattering events while the lower points come mainly from the π^0 background.

Using the same experimental arrangement it was also possible to study the reaction $\vec{\gamma}+{}^4\mathrm{He}\rightarrow\pi^0+{}^4\mathrm{He}$ [21,22]. A schematic view of the detector geometry is shown in Fig. 1.

III. DATA ANALYSIS

The main features of the data analysis were as follows: (i) Events were selected to belong to the main peak of the tagger TOF spectrum, which corresponded to *true* coincidences between the incoming photon and the detected nuclear event. (ii) Charged particles detection was suppressed rejecting all events in which energy signals higher than 3 MeV were deposited in the front detector. (iii) Cosmics were suppressed by rejecting events where multiple signals were recorded in the *annulus* detector with a total deposited energy of more than 40 MeV. (iv) Background from coherent π^0 photoproduction on ^{4}He was initially reduced by selecting only those events that provided either no signal in the *C* bars or a signal in the electronic noise range.

The bi-dimensional plot of the energy of the scattered photon versus the energy of the incoming photon is plotted in Fig. 2 for all the events that matched the described selection. The Compton events appear as a clear upper band, well separated from the lower points, that are mainly due to π^0 photoproduction.

To perform a clear rejection of the residual π^0 background, the difference between the energy measured by the NaI(Tl) detector and the theoretical energy computed for photons scattered in a Compton process was calculated. The peak around the zero value corresponded to Compton events and was fitted with a Gaussian curve. Its integral provided the total amount of detected Compton events. The result of the integration was different from the result of events counting by less than 1%. This technique provided a clear procedure also in those few cases where some tail from π^0 background would slightly overlap the Compton peak [21].

Accidental and background events were rejected applying the same selection as described above to events which were not recorded at the main tagger TOF peak and to empty targets events. Those events which survived the analysis criteria were normalized according to the incoming tagged photon flux and subtracted. All geometrical acceptances, corrections for detector efficiencies and thresholds were modeled with a Monte Carlo simulation based on GEANT 3.21 [25], duplicating all the constraints imposed in the analysis procedure.

The experimental cross sections have been computed for each polarization state using the following relation:

$$\left(\frac{d\sigma}{d\Omega}\right)_{\mathrm{expt.}}=\frac{N_C A}{N_\gamma \varrho l N_A \varepsilon \Delta\Omega}, \tag{2}$$

where N_C is the number selected Compton events, N_γ is the number of incoming tagged photons, N_A is the Avogrado constant, A is the ^{4}He mass number, l and ϱ are the length and the density of the target, respectively, $\Delta\Omega$ is the solid angle covered by the NaI(Tl) detector, and ε is the detection efficiency. The total systematic uncertainty in the final cross-section results is estimated to be 3%. Comparison of data taken at the same photon energy of 224 MeV but with different laser lines (and hence different beam polarization and tagged flux) yielded a χ^2 per point with respect to the mean of 0.66.

IV. RESULTS

Final results of unpolarized differential cross sections are shown in Fig. 3 as full triangles, together with existing data.

The points shown as full circles at θ_γ=0° have been calculated from the total photoabsorption cross section data [26] in a model independent way. The optical theorem fixes the imaginary part of the forward amplitude $\mathrm{Im}(f(E_\gamma,0°))$,

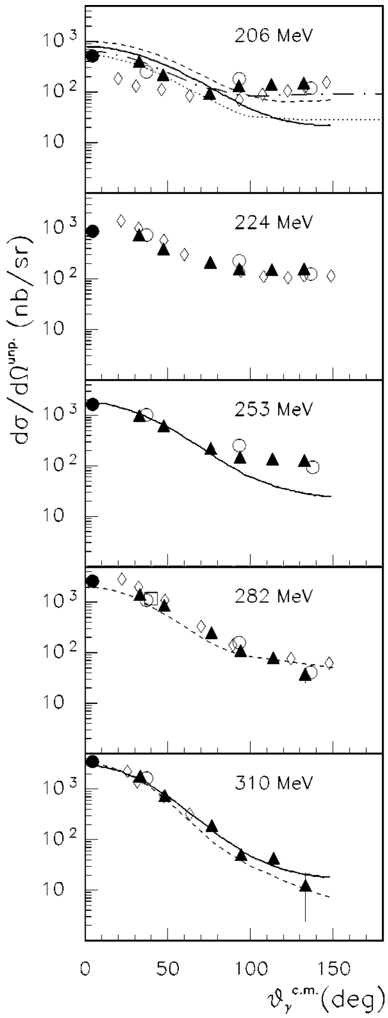

FIG. 3. Unpolarized differential cross sections. Solid triangles are from this measurement, and solid circles at 0° are deduced from photon total absorption cross section—see text. Cross sections from Refs. [17,16] at 187, 235, 280, and 320 MeV are plotted as open diamonds in the 206, 224, 282, and 310 MeV panels, respectively. A measurement from Ref. [20] at 280 MeV is shown as an open square. Mainz data from Ref. [14] are plotted as open circles. The predictions of Δ-hole calculations are shown as bold solid [13] and short-dashed [8] curves. Dash-dotted and dotted curves in the upper panel are calculations from a recent schematic model [5] including I.A. and I.A.+MEC contributions, respectively.

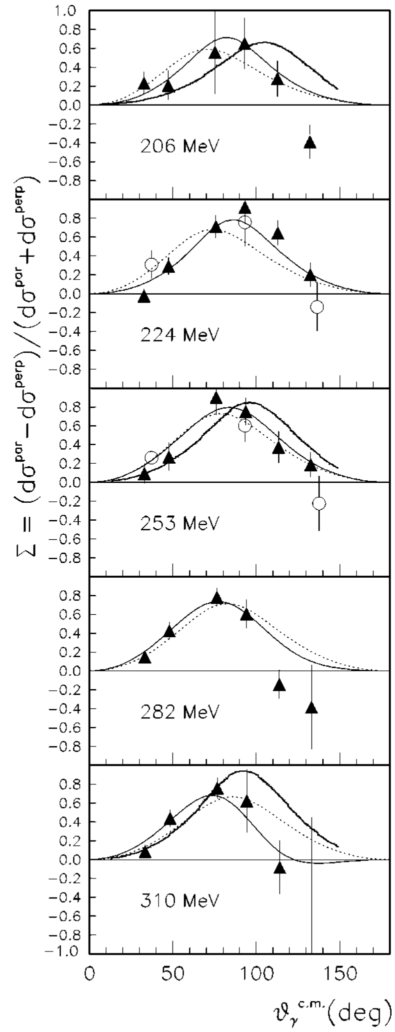

FIG. 4. Linear polarization asymmetries Σ. Solid triangles are from this measurement, Mainz data from Ref. [14] are plotted as open circles. Δ-hole calculations from Ref. [13] are shown as bold solid curves. Dotted and thin solid curves are multipole fits to the data including dipole and dipole plus quadrupole terms, respectively.

$$\mathrm{Im}(f(E_\gamma, 0°)) = \frac{E_\gamma}{4\pi\hbar c}\sigma(E_\gamma), \tag{3}$$

where E_γ is the incoming photon energy and $\sigma(E_\gamma)$ is the total photon absorption cross section. The real part of $f(E_\gamma, 0°)$ is related to the values of $\sigma(E_\gamma)$ at all energies through the subtracted Kramers-Kronig dispersion relation [27],

$$\mathrm{Re}[f(E_\gamma, 0°) - f(0, 0°)] = \frac{E_\gamma^2}{2\pi^2\hbar c}P\int_0^\infty dE' \frac{\sigma(E')}{E'^2 - E_\gamma^2}, \tag{4}$$

where $f(0, 0°) = -(Z^2e^2)/(M_A c^2)$ is the Thomson limit and M_A is the nuclear mass.

Figure 4 shows the results for linear polarization beam asymmetries $\Sigma = \sigma_\parallel - \sigma_\perp / \sigma_\parallel + \sigma_\perp$ as solid triangles. The few existing data from Ref. [14] are also plotted as open circles.

The same experimental results are also shown as triangles in Figs. 5 and 6 in terms of the cross sections measured with the electric vector of the incident photon parallel ($\sigma_\parallel$) and perpendicular ($\sigma_\perp$) to the scattering plane, respectively. The open circles are deduced from Ref. [14]. All results are also reported in Table I as a function of the photon scattering angle in the center of mass reference frame $\theta_\gamma^{\mathrm{c.m.}}$.

Multipole fit

Our final dataset consists of 60 measurements (30 points for each of the observables $\sigma_\parallel$ and $\sigma_\perp$) and, together with 5 values for the differential cross sections at $\theta_\gamma = 0°$, may be considered the first database obtained with polarized photons which is wide enough to attempt a multipole analysis in the energy range of the Δ resonance.

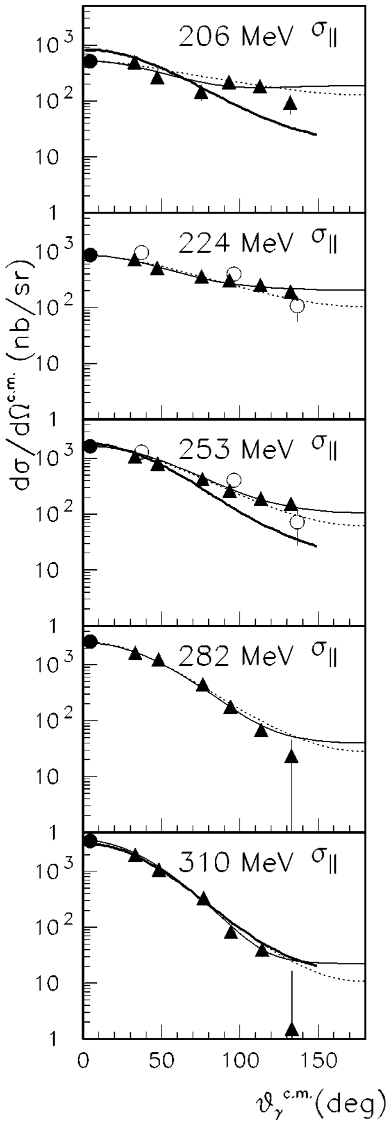

FIG. 5. Cross sections for ^{4}He$(\vec{\gamma},\gamma)$ for photon polarizations parallel to the scattering plane, $\sigma_\parallel$. Triangles are from this measurement; circles at 0° are deduced from total photon absorption cross section—see text. The Mainz data [14] at 230 and 250 MeV are plotted as open circles in the 224 and 253 MeV panels, respectively. Bold solid curves are from Δ-hole calculations [13]. Dotted and thin solid curves are multipole fits to the data including dipole and dipole plus quadrupole terms, respectively.

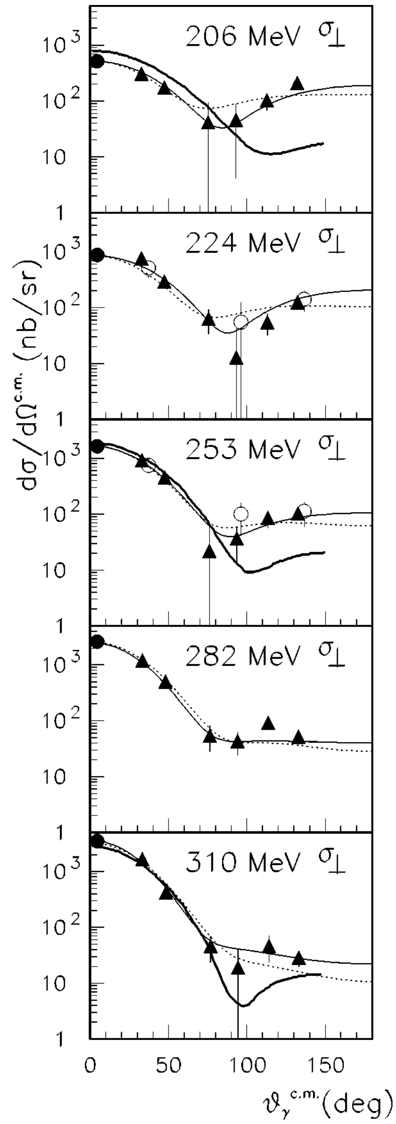

FIG. 6. Cross sections for ^{4}He$(\vec{\gamma},\gamma)$ for photon polarizations perpendicular to the scattering plane, $\sigma_\perp$. Data symbols and curves follow the same notations as defined in Fig. 5.

In the case of Compton scattering on spin-zero nuclei, the differential cross sections with polarized photons in the c.m. reference frame may be expressed in terms of helicity nonflip $[T^{11}(k,\theta_\gamma^{\text{c.m.}})]$ and flip amplitudes $[(T^{1-1}(k,\theta_\gamma^{\text{c.m.}})]$ as follows [13]:

$$\frac{d\sigma}{d\Omega}=\left(\frac{M_A}{E_{\text{c.m.}}}\right)^2|T^{11}|^2+|T^{1-1}|^2,$$

$$\hat{\Sigma}=-\left(\frac{M_A}{E_{\text{c.m.}}}\right)^2 2\,\text{Re}[T^{11}(T^{1-1})^*] \tag{5}$$

where $E_{\text{c.m.}}=\sqrt{s}$ is the total c.m. energy, k is the photon energy in the c.m. reference frame, and $\theta=\theta_{\text{c.m.}}$ is the c.m. photon scattering angle. For $\sigma_\parallel$ and $\sigma_\perp$ the equivalent relations are the following:

$$d\sigma_\parallel=\left(\frac{M_A}{E_{\text{c.m.}}}\right)^2|T^{11}-T^{1-1}|^2,$$

$$d\sigma_\perp=\left(\frac{M_A}{E_{\text{c.m.}}}\right)^2|T^{11}+T^{1-1}|^2. \tag{6}$$

The amplitudes $T^{1\pm1}(k,\theta_\gamma^{\text{c.m.}})$ may be expanded in terms of the complex *generalized polarizabilities* $EL(k)$ and $ML(k)$ as follows [13,28]:

$$T^{1\pm1}(k,\theta_\gamma^{\text{c.m.}})=\sum_L\frac{(-1)^{L+1}}{\sqrt{2L+1}}d^L_{1\pm1}(\theta_\gamma^{\text{c.m.}})[EL(k)\pm ML(k)] \tag{7}$$

where $d^L_{1\pm1}$ are the rotation matrix elements between states of angular momentum $\langle L,1|$ and $|L,\pm1\rangle$.

TABLE I. Differential cross sections $d\sigma/d\Omega$ and beam asymmetries Σ as a function of the photon scattering angle in the center of mass reference frame $\theta_\gamma^{\mathrm{c.m.}}$. The same results are also expressed in terms of the differential cross sections measured with the electric vector of the incident photon parallel ($d\sigma_\parallel$) and perpendicular ($d\sigma_\perp$) to the scattering plane. Statistical errors are tabulated in brackets.

$\theta_\gamma^{\mathrm{c.m.}}$(deg)	$\frac{d\sigma}{d\Omega}$ (nb/sr)	Σ	$d\sigma_\parallel$ (nb/sr)	$d\sigma_\perp$ (nb/sr)
		E_γ=206 MeV		
33	400 (45)	0.23 (0.12)	494 (71)	308 (63)
47	220 (32)	0.21 (0.16)	267 (50)	174 (44)
75	95 (34)	0.56 (0.44)	148 (49)	42 (51)
93	132 (31)	0.65 (0.27)	218 (50)	46 (42)
113	143 (26)	0.28 (0.19)	182 (39)	102 (35)
132	151 (24)	−0.39 (0.18)	93 (35)	210 (35)
		E_γ=224 MeV		
33	749 (48)	−0.023 (0.075)	732 (78)	764 (69)
47	398 (36)	0.29 (0.09)	516 (60)	291 (47)
76	215 (26)	0.71 (0.12)	366 (45)	64 (31)
93	158 (18)	0.92 (0.18)	305 (29)	13 (30)
113	153 (18)	0.64 (0.13)	255 (31)	55 (24)
132	158 (18)	−0.20 (0.13)	193 (29)	124 (26)
		E_γ=253 MeV		
33	1005 (86)	0.09 (0.1)	1100 (140)	910 (130)
48	630 (78)	0.27 (0.15)	800 (120)	460 (120)
76	223 (30)	0.90 (0.18)	424 (48)	22 (45)
94	150 (16)	0.75 (0.14)	263 (27)	37 (24)
113	138 (19)	0.37 (0.17)	188 (26)	86 (31)
133	128 (14)	0.19 (0.13)	152 (20)	104 (23)
		E_γ=282 MeV		
33	1424 (83)	0.15 (0.06)	1640 (130)	1210 (120)
48	880 (74)	0.42 (0.09)	1250 (120)	506 (97)
76	250 (23)	0.78 (0.10)	446 (39)	54 (26)
94	111 (14)	0.60 (0.15)	178 (21)	44 (20)
114	80 (12)	−0.14 (0.15)	69 (16)	92 (19)
133	38 (13)	−0.38 (0.45)	23 (22)	52 (16)
		E_γ=310 MeV		
33	1821 (92)	0.084 (0.056)	1975 (140)	1670 (140)
48	749 (67)	0.44 (0.09)	1080 (110)	419 (83)
77	193 (22)	0.76 (0.11)	339 (39)	46 (23)
94	51 (13)	0.62 (0.34)	83 (20)	19 (20)
114	43 (12)	−0.08 (0.28)	40 (10)	47 (23)
133	12 (10)	−1.2 (1.7)	1.53 (15)	29 (9)

Limiting the expansion to the quadupole order, in the impulse approximation, the parallel and perpendicular cross sections are simply given by the following relations:

$$d\sigma_\parallel = \left(\frac{M_A}{E_{\mathrm{c.m.}}}\right)^2 |F(q^2)|^2 \left| \frac{1}{\sqrt{3}}\overline{E}1 \cos\theta + \frac{1}{\sqrt{3}}\overline{M}1 - \frac{1}{\sqrt{5}}\overline{M}2 \cos\theta - \frac{1}{\sqrt{5}}\overline{E}2(2\cos^2\theta - 1)\right|^2, \tag{8}$$

$$d\sigma_\perp = \left(\frac{M_A}{E_{\mathrm{c.m.}}}\right)^2 |F(q^2)|^2 \left| \frac{1}{\sqrt{3}}\overline{M}1 \cos\theta + \frac{1}{\sqrt{3}}\overline{E}1 - \frac{1}{\sqrt{5}}\overline{E}2 \cos\theta - \frac{1}{\sqrt{5}}\overline{M}2(2\cos^2\theta - 1)\right|^2, \tag{9}$$

where $\overline{E}L(k)$ and $\overline{M}L(k)$ describe the multipole interaction at the nucleon level, $F(q^2)$ is the nuclear form factor which originates from the coherent sum of the contributions of the single nucleons, with q being the c.m. momentum transferred to the nucleus. Improving the model beyond the impulse approximation would require more complicated expressions for the generalized polarizabilities, also including two-body form factors, and would require a much higher number of free parameters in a multipole fit.

We used the last two expressions to attempt a phenomenological multipole analysis with the aim of investigating the role of contributions beyond the leading dipole multipoles. An initial set of χ^2 minimizations was performed using data at fixed beam energies. These were used both to infer the energy dependence of the generalized polarizabilities coefficients and to initialize a global energy dependent fit of all the data. The amplitudes were parametrized as a function of the incoming laboratory photon energy E_γ, using a Breit-Wigner for the resonant $\overline{M}1$ multipole (defined by three parameters) and a linear dependence for the real and imaginary parts of the other three multipoles (each additional multipole is defined by four parameters). The following form factor was used:

$$|F(q^2)|^2 = e^{-r^2q^2/3} = e^{-2/3r^2k^2(1-\cos\theta_{\mathrm{c.m.}})}, \tag{10}$$

where r is an additional free parameter. The previous expression has been chosen similar to the nuclear form factor measured in electron scattering, which provides the Fourier transform of the charge distribution. In the electron scattering case the parameter $r=\sqrt{\langle r_N^2\rangle}=1.67$ fm is the root mean square (r.m.s.) radius of the charge distribution [30,31]. In the case of Compton scattering the absorption and the emission of the photon do not necessarily take place in the same point in space time and the nuclear form factor may be compared with the so-called *mass*-form factor, given by the ratio of the form factor in electron scattering and the dipole proton form factor. The r.m.s. radius of this modified distribution is 1.4 fm.

A series of tests were carried out by starting with a fit of the $\overline{M}1$ amplitude only and subsequently adding the $\overline{E}1$, $\overline{E}2$, and $\overline{M}2$ contributions. At each step an F test was used to verify the statistical significance of the improvement from additional terms [29].

Considering only dipole terms in Eqs. (8) and (9), it was possible to reproduce the data with a χ^2/ν=2.2 and the corresponding fits are shown in Figs. 4–6 as dotted curves. The full analysis including $\overline{E}2$ and $\overline{M}2$ scattering provides a final χ^2/ν=1.5 and it corresponds to the thin solid curves in Figs. 4–6. The largest effect is given by the contribution of $\overline{M}2$ and its interference with the other multipoles. Additional improvements are obtained for the location of the minima of

$\sigma_\perp$, which corresponds to the maxima of the asymmetry Σ. Moreover the general trend of the fitted curves at backward angles are closer to the data, especially at lower energies. The average of the results for the parameter r, obtained in the different fits, is r=1.36±0.08 fm, comparable with the $\sqrt{\langle r_N^2 \rangle}$ of the previously quoted mass-form factor.

V. DISCUSSION AND CONCLUSIONS

The present experiment is the first systematic study of the Compton scattering with polarized photons on ^{4}He. The existing database in the same energy range contained only nine asymmetry measurements with large error bars [14], and it is now extended by more than a factor three. Figures 3–6 show the comparison among the present results and the existing measurements at comparable incoming photon energies. Good agreement is found within the error bars but the trend of the angular distribution is now much improved.

Results for the unpolarized differential cross section are also compared with two different versions of the Δ-hole model [8,13], shown in Fig. 3 as short dashed and bold solid curves, respectively. The Δ-hole model attempts to describe pion-scattering, pion photoproduction, and photon scattering in a unified approach, assuming that the γ-nucleus interaction occurs through the formation of Δ-hole states which propagate inside the nucleus. The influence of the nuclear medium to the Δ-isobar characteristics, due to kinematical effects such as Fermi motion, Pauli blocking of Δ decay, $\Delta-N$ binding, multiple scattering of intermediate pions, and coupling of the Δ to π absorption channels, are introduced by modifications of a Δ-hole propagator, defined for all coherent processes. None of the Δ-hole calculations [6–13] include scattering from intermediate mesons.

The most important discrepancies appear at backward angles and lower energies. For the lowest energy bin (206 MeV) some improvement is obtained by a model where MEC contributions are added to the one-body terms (I.A.) [5] (dot-dashed curve).

Predictions from Pasquini and Boffi [13] are also available for the polarization dependent part of the differential cross section and are also plotted as bold solid curves in Figs. 4–6. This model provides a good description of the cross section for incoming photon energies close to the Δ peak, but it is not able to reproduce the rise at backward angles and the magnitude at lower energies and forward angles. As it has been already noticed in Ref. [14], one of the main reasons for the failure is due to the fact that the background nonresonant processes are not accurately taken into account. The inclusion of the effects of two-body currents and medium corrections to the nonresonant $\overline{E}1$ multipole from seagull term and Kroll-Ruderman contributions provides an improvement at lower energies and forward angles, but strong discrepancies remain at backward angles [14].

Scattering at large angles corresponds to high momentum transfer and it is sensitive to the details of the reaction. It has been suggested that the existing disagreement among all theoretical calculations and experimental results is due to some missing mechanism [5]. This may be expressed by also saying that the $\overline{M}1$ and the $\overline{E}1$ multipole contributions are not sufficient to reproduce the experimental dynamics, while all theoretical calculations [8,13,14,5] were limited to dipole scattering. Although at these energies $\overline{M}1$ transitions through the Δ resonance dominate the elementary amplitude for scattering from nucleons, when transformed into nuclear coordinates this strength is expected to spread into higher multipoles.

Comparison with results from a phenomenological multipole fit is shown in Figs. 4–6, where contribution from dipole terms and dipole plus quadrupole terms are plotted as dotted and thin solid curves, respectively. Finite size effects are introduced by means of a one-body nuclear form factor with a free radius parameter r whose value, extracted from the data, is compatible with results obtained for the *mass*-form factor which is about 20% smaller than the corresponding (e,e) value.

Dipole contributions already provide the general trend of the data and the form factor helps the convergence of the multipole expansion by taking higher multipoles into account in an approximate way.

Nonetheless, explicit quadrupole terms are necessary to reproduce the correct behavior at backward angles and the position of the minimum for $\sigma_\perp$.

In conclusion, the present work provides a significant contribution to the existing experimental information on polarization observables in Compton scattering on ^{4}He. Comparison with existing theoretical models confirms that medium effects of Δ-hole models are not enough to reproduce the elastic scattering of polarized photons in the intermediate energy region.

Only dipole scattering has been included in existing microscopic calculations, and our analysis suggests that higher multipole terms could provide significant additional improvements.

ACKNOWLEDGMENTS

The authors are grateful to Barbara Pasquini for fruitful discussion. This work has been supported by the Italian Istituto Nazionale di Fisica Nucleare, the U.S. Department of Energy, under Contract No. DE-AC02-76-CH00016 and the U.S. National Science Foundation.

[1] D. Drechsel, O. Hanstein, S. S. Kamalov, and L. Tiator, Nucl. Phys. **A645**, 145 (1999).

[2] F. Rambo *et al.*, Nucl. Phys. **A660**, 69 (1999).

[3] A. I. L'vov and V. A. Petrun'kin, Lect. Notes Phys. **365**, 123 (1990).

[4] V. A. Petrun'kin and A. I. L'vov, *Proceedings of the 8th International Seminar on Electromagnetic Interactions of Nuclei at Low and Medium Energies, Moscow, 1991* (Institute for

Nuclear Research, Moscow, 1992), p. 109.
[5] M.-Th. Hutt, A. I. L'vov, A. I. Milstein, and M. Schumacher, Phys. Rep. **323**, 457 (2000).
[6] W. Weise, Nucl. Phys. **A358**, 163 (1981).
[7] E. Oset and W. Weise, Nucl. Phys. **A368**, 375 (1981).
[8] J. H. Koch, E. J. Moniz, and N. Ohtsuka, Ann. Phys. (Leipzig) **154**, 99 (1984).
[9] J. Vesper, D. Drechsel, and N. Ohtsuka, Nucl. Phys. **A466**, 652 (1987).
[10] E. Oset and L. L. Salcedo, Nucl. Phys. **A468**, 631 (1987).
[11] C. Garcia-Recio, E. Oset, L. L. Salcedo, D. Strottman, and M. J. Lopez, Nucl. Phys. **A526**, 685 (1991).
[12] B. Korfgen *et al.*, Phys. Rev. C **50**, 1637 (1994).
[13] B. Pasquini and S. Boffi, Nucl. Phys. **A598**, 485 (1996).
[14] A. Kraus *et al.*, Phys. Lett. B **432**, 45 (1998).
[15] E. J. Austin *et al.*, Phys. Rev. Lett. **57**, 972 (1986).
[16] E. J. Austin *et al.*, Phys. Rev. Lett. **61**, 1922 (1988).
[17] D. Delli Carpini *et al.*, Phys. Rev. C **43**, 1525 (1991).
[18] J. P. Miller *et al.*, Nucl. Phys. **A546**, 199c (1992).
[19] R. Igarashi *et al.*, Phys. Rev. C **52**, 755 (1995).
[20] O. Selke *et al.*, Phys. Lett. B **369**, 207 (1996).
[21] M. Capogni, Ph.D. thesis, University of Rome "Tor Vergata," 1998.
[22] V. Bellini *et al.*, Nucl. Phys. **A646**, 55 (1999).
[23] D. Moricciani *et al.*, Few-Body Syst., Suppl. **9**, 349 (1995).
[24] C. E. Thorn *et al.*, Nucl. Instrum. Methods Phys. Res. A **285**, 447 (1989).
[25] GEANT Detector Description and Simulation Tool, CERN Program Library Long Writeup W5013, CERN, Geneva, 1993.
[26] M. MacCormick *et al.*, Phys. Rev. C **55**, 1033 (1997).
[27] M. Gell-Mann, M. Goldberger, and W. Thirring, Phys. Rev. **95**, 1612 (1954); H. Alvensleben *et al.*, Phys. Rev. Lett. **30**, 329 (1973).
[28] H. Arenhoevel and W. Greiner, Prog. Nucl. Phys. **10**, 167 (1969); J. Vesper, D. Drechsel, and N. Ohtsuka, Nucl. Phys. **A466**, 652 (1987).
[29] P. R. Bevington, *Data Reduction and Error Analysis for the Physical Sciences* (McGraw-Hill, New York, 1969)
[30] L. R. B. Elton, *Nuclear Sizes* (Oxford University Press, New York, 1961).
[31] C. R. Ottermann *et al.*, Nucl. Phys. **A436**, 688 (1985).